Polímeros
ISSN 1678-5169 (Online)

https://doi.org/10.1590/0104-1428.20220087

ORIGINAL ARTICLE

Crystallization and fusion kinetics of Poly(butylene terephthalate)/Titanium Dioxide

José Vinícius Melo Barreto[1], Antônio Anderson da Silva Gomes[1], Amanda Meneses Araújo[1], Andreas Ries[2], Janetty Jany Pereira Barros[3]* and Renate Maria Ramos Wellen[1,3]

[1]Departamento de Engenharia de Materiais, Universidade Federal da Paraíba – UFPB, João Pessoa, PB, Brasil

[2]Centro Multidisciplinario de Investigaciones Tecnológicas, Universidad Nacional de Asunción, Campus Universitario San Lorenzo, San Lorenzo, Paraguay

[3]Unidade Acadêmica de Engenharia de Materiais, Universidade Federal de Campina Grande – UFCG, Campina Grande, PB, Brasil

**janetty_b@hotmail.com*

Abstract

In this paper, the crystallization, fusion, and activation energy (Ea) of PBT/TiO_2 were thoroughly evaluated using DSC. Increasing the rates shifted the peaks of melt crystallization to lower temperatures while the fusions were almost unaffected. TiO_2 hindered the melt crystallization of PBT and lower crystallization rates, i.e., CMAX and K' were acquired, in general, the crystallinity degree (Xc) was 4% higher in PBT/TiO_2 which is in the marginal error. Pseudo-Avrami and Mo models were applied to evaluate the melt crystallization kinetics; both fitted the melt crystallization quite well; deviations were observed at the beginning and the crystallization end most due to the nucleation and spherulites impingement during the secondary crystallization. Ea was evaluated using the Friedman model, considering the values of Ea less energy has to be removed from PBT/TiO_2 when compared to PBT, specifically at 1% of TiO_2.

Keywords: *activation energy, kinetics, PBT, phase transition, TiO_2.*

How to cite: Barreto, J. V. M., Gomes, A. A. S., Araújo, A. M., Ries, A., Barros, J. J. P., & Wellen, R. M. R. (2023). Crystallization and fusion kinetics of Poly(butylene terephthalate)/Titanium Dioxide. *Polímeros: Ciência e Tecnologia*, *33*(1), e20230006. https://doi.org/10.1590/0104-1428.20220087

1. Introduction

Polyesters are plastic resins widely used in sundry industrial applications, from the general goods as commodities to the sophisticated products with high technological performance and added value. These resins contribute for almost 18% of the world's polymer production[1]. Among them, one of the most important is poly(butylene terephthalate) (PBT), a thermoplastic, semi-crystalline with excellent processing properties. Its high chemical, thermal and mechanical performances make PBT a potential candidate for many applications in science and technology[2-7].

Literature has reported the crystallization kinetics of PBT upon additives and fillers addition, the second phase addition may promote the heterogeneous nucleation and reduce the crystallization time, speeding up its general processing[8]. However, other properties can be achieved, such as significant improvement in the mechanical properties[9], antistatic and super-strength characters[10] are examples of synergistic PBT compounds, filled with aluminum oxide (Al_2O_3), epoxide elastomers and carbon nanotubes, for instance.

In order to improve polymers' properties, additives and fillers are commonly added. For instance, Titanium dioxide (TiO_2) which is used due to its high thermal and chemical stability, non-toxicity, photo-catalytic character and antibacterial action, for instance[11,12], the addition of TiO_2 to the compounds may increase the solar reflectance[13], rigidity[14], tenacity[15], synthesize films[16] and increases the degree of crystallinity[17]. Due to these great achievements, adding TiO_2 can be attractive aiming at higher PBT performance, therefore in this work, PBT was doped with TiO_2, in amounts ranging from 0 to 10% of the weight. Afterwards, the phase transitions, i.e., crystallization and melting were investigated.

Zhou et al.[18] reported TiO_2 effect in nanocomposites of poly(butene 2,5-furan dicarboxylate) (PBF), a biological-based polyester similar to PBT, at concentrations up to 7% of the weight; TiO_2 acted as a nucleating agent accelerating the crystallization as well as improving UV resistance. In the present work, as later on discussed at low PBT/TiO_2 contents (1% wt) there was no nucleating effect, suggesting that the deterrent effect of TiO_2's solid particles was greater than the nucleation ability into PBT matrix during the melt crystallization[5], investigation of the crystallization kinetics and energetic measurements are presented contributing to scientific and technological databases.

Crystallization and fusion of PBT and PBT/TiO_2 composites were recorded using differential scanning calorimetry (DSC)

through non-isothermal scans, and applying several heating/cooling rates. Crystallization kinetics was evaluated using Pseudo-Avrami and Mo models, measured discrepancies are provided validating the modeling. Additionally, this work reports the activation energy evaluations for crystallization and fusion processes, a methodology rarely reported. The activation energy for the melt crystallization was computed using the Friedman isoconversional model[19]. Regarding the activation energy of fusion, Toda et al.[20] suggested a model for polymer fusion, considering the geometry of melting cylindrical rods, however, the literature reports that for cases of sample overheating during fusion, the most robust isoconversional models for calculation of the crystallization activation energy are also suitable for the evaluation of the activation energy of the fusion, therefore Friedman's isoconversional method was applied in this work[21]. Based on our database, the kinetics of crystallization and its modeling discrepancies, as well as the activation energies evaluation for PBT/TiO_2, have been rarely reported for polymers composites.

2. Materials and Methods

2.1 Materials

PBT 195 Valox was supplied by Sabic company (Bergen op zoom Netherlands), with density of 1.31 g cm^{-3}. TiO_2 was purchased from Evonik Degussa Co. with surface area of 50 m^2/g and a 75:25 ratio of anatase and rutile, with an average crystal size of 25 to 94 nm.

2.2 Compounding

PBT compounds with 1, 5, and 10% of the weight of TiO_2 were prepared in a Haake Rheomix 600 (Germany) laboratory internal mixer fitted with high-intensity rotors type rollers, at 240 °C, 60 rpm during 10 min.

2.3 Scanning electron microscopy (SEM)

Scanning electron microscopy images were captured using a LEO 1430 unit, from Zeiss (USA). The specimens were previously fractured in liquid nitrogen to avoid plastic deformation, afterwards, coated with a carbon layer aiming to avoid the charges accumulation.

2.4 Differential scanning calorimetry

The phase transitions, i.e., crystallization and fusion, as well as the thermal properties were monitored with a DSC Q20 from TA Instruments (USA). Specimens weighing approximately 3 mg were experimented in closed aluminum pans under nitrogen gas flow of 50 mL/min. The applied thermal cycle consisted of: heating from 25 °C to 270 °C, isotherm at 270 °C for 3 minutes, cooling from 270 °C to 20 °C and re-heating from 20 °C to 270 °C using constant heating/cooling/reheating rates of 5, 10, 20, and 30 °C/min. Figure 1 displays a typical DSC scan together with an applied thermal cycle illustrated as a dotted red line. The investigated phase transitions are presented and coded as F_1: first fusion; C_1: melt crystallization; and F_2: second fusion.

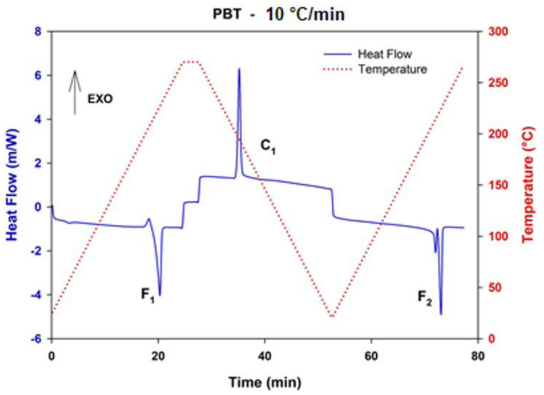

Figure 1. Typical DSC scan for PBT collected during applied thermal cycles with the heating/cooling/re-heating of 10 °C/min. The dotted red line is the applied thermal program. The solid blue line the heat flow signal with the investigated phase transitions, i.e., F_1, C_1, and F_2.

2.5 Integration and conversion during crystallization and fusion measurements

The crystallizable mass conversion during crystallization or fusion, x = x (t), was estimated using Equation 1, through the energy flow between the starting and ending points previously defined.

$$x(t)=\frac{1}{Eo}\int_{t_1}^{t}\left|J(t')-(t')\right|dt' \quad (1)$$

where: J is the heat flow of the phase transition and t' the time for partial conversion; J_0 is an adequate baseline and E_0 (Equation 2) refers to the total exchanged heat between the specimen and the neighborhood during the event[22].

$$E_0=\int_{t_1}^{t_2}\left|J(t)-J_0(t)\right|dt \quad (2)$$

the crystallization or fusion rate c = c (t) was computed using Equation 3[22].

$$c(t)=\frac{dx}{dt}=\frac{\left|J(t)-J_0(t)\right|}{E_0} \quad (3)$$

The degree of crystallinity X_c developed during the event was evaluated using Equation 4:

$$X_c=\frac{\Delta H}{\Delta H_m^0}*100\ (\%) \quad (4)$$

In this work, the equilibrium melting enthalpy used for PBT was 140 J/g and the equilibrium melting temperature was $T_m^0=226°C$[23].

3. Results and Discussions

3.1 Scanning electron microscopy image (SEM)

Figure 2 shows SEM image of PBT/10% TiO_2 where the white dots are TiO_2 which are well dispersed in PBT

matrix as a result of the proper compounding parameters. The applied magnification was 10.000 x.

3.2 Melt crystallization (C1) measurements

Relative crystallinity (X_{rel}) and crystallization rate (dx/dt) as temperature functions for PBT and PBT/1% TiO_2 using the investigated cooling rates are displayed in Figure 3. The Supplementary Material presents plots for PBT/5% TiO_2, and PBT/10% TiO_2 (please see Figure S3 and S4).

Sigmoidal behavior was verified for X_{rel} plots in Figure 3a and 3b characterizing the phase transition without discontinuities, commonly observed in polymers[24]. The $d\alpha/dt$ showed bell shape, increasing at the beginning of crystallization which is related to nucleation and primary crystallization, reaching the top and decreasing afterwards configuring the secondary crystallization and spherulites impingement[25].

Sigmoids obtained from the higher cooling rates are displaced to lower temperatures due to the time effect, i.e., upon higher cooling rates exists less time for the nucleation, and crystal growth occurs at lower temperatures[26]. The crystallization rates increase for the higher cooling rates as may be confirmed from the heights of the bell-shaped curves. Quantitative data for the crystallization rates is tabled in the Supplementary Material (Table S1). Concerning the TiO_2 addition in general, sigmoids of PBT/TiO_2 were displaced to lower temperatures, nevertheless, the filler effect is nonlinear, and this topic is further discussed in terms of activation energy.

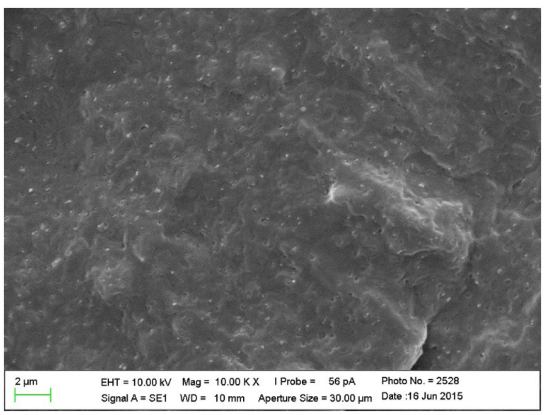

Figure 2. Scanning electron microscopy image of PBT/10% TiO_2, as obtained after compounding

3.3 First (F1) and second (F2) fusion measurements

Figure 4a and b presents the sigmoids collected for F_1 and F_2, respectively, the corresponding melting rates are also shown within the plots. In general, the fusion is less sensitive to the heating rates and TiO_2 addition which is evidenced as subtle bell peaks displacement. During the first fusion, both compounds presented quite similar melting rates and molten fraction profiles, light dissimilarity was verified for PBT/ 10% TiO_2 that melted in a lower temperature range. The readers may find additional molten fraction plots in the Supplementary Material, please see Figure S2 and Figure S8.

Regarding F_2, the investigated compounds presented quite similar sigmoid and melting profiles, nevertheless, contrarily to F_1, F_2 peaks displayed complex character which may be linked to distinct morphologies and crystals perfection[27]; it seems there are smaller/imperfect crystals that melt in the temperature range from 200 to 220 °C while the most perfect/bigger melt between 220 and 240 °C[28,29]. It is supposed there was crystal reordering during the melt crystallization and second heating which promoted the development of higher perfected crystals, similar trend is reported in the literature for PP, PET, Nylon 1212[30-32], for instance. Apparently, TiO_2 addition did not significantly change the F_2 trend, however during F_2 higher melting rates were verified suggesting easier melting, deeper discussion related to this topic and its relationship with the activation energy for melting is further on presented.

The degrees of crystallinity computed for F_1 and F_2 are displayed in Figure 5. In general, X_c decreased with increasing the heating rate, specifically for the heating rates higher than 10 °C/min, since for higher heating rates there is reduced time for the crystal formation. The thermal environment changes rapidly hindering or interfering in the crystals' nucleation and growth, hence producing shorter or imperfect crystallites[33].

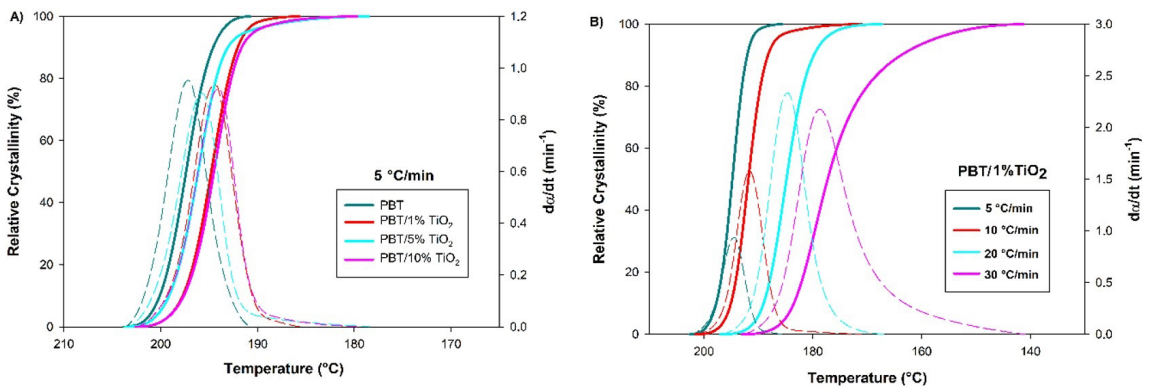

Figure 3. Plots for the relative crystallinity (solid line) and crystallization rate (dashed line) as temperature function. (A) Fixed cooling rate of 5 °C/min and (B) composition of 1% de TiO_2 cooled at different rates.

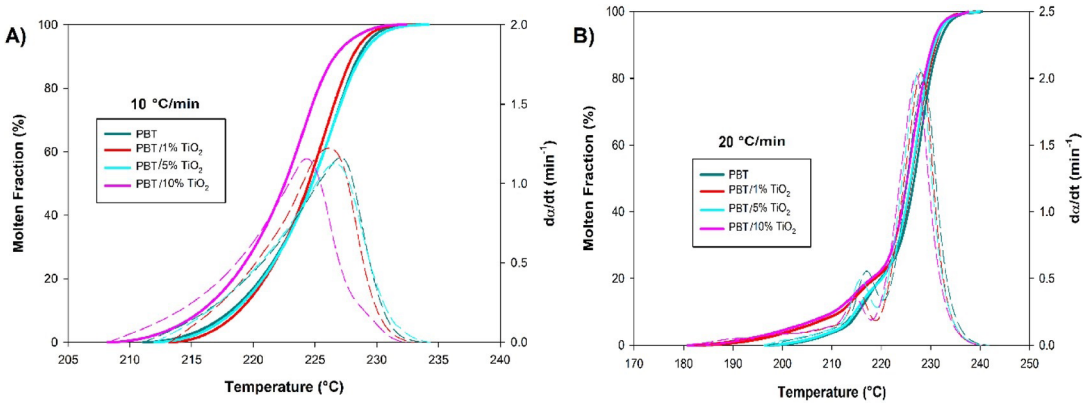

Figure 4. Plots for the molten fraction (solid line) and melting rates (dashed line) as temperature function. (A) First fusion at 10 °C/min and (B) second fusion at 20 °C/min.

Regarding TiO_2 addition, the composites presented a slight increase in Xc, i.e., approximately 4% higher.

3.4 Melt crystallization kinetics – Pseudo Avrami

Aiming to further analyzing the non-isothermal melt crystallization, the kinetics of crystallization of neat PBT and PBT/TiO_2 composites was analyzed. The relative crystallinity as crystallization time function was computed as the exothermic peak areas ratio using Equation 5:

$$X_{rel} = \frac{\int_0^t \left(\frac{dH_c}{dt}\right) dt}{\int_0^\infty \left(\frac{dH_c}{dt}\right) dt} \quad (5)$$

where: $\frac{dH_c}{dt}$ is the released heat; X_{rel} is the relative crystallinity measured from the peak integration as the ratio between the total and partial peak's area, t_0 and t_∞ are the onset and end melt crystallization times.

3.5 Pseudo-Avrami modeling

Avrami[33-37] developed a macrokinetic model to investigate the isothermal crystallization, based on microkinetics approaches. The Avrami model considers the relative crystallinity x as time function τ computed in the event starting according to Equation 6:

$$x = 1 - exp\left(-K\tau^n\right) \quad (6)$$

K = K(T) and n = n(T) are the Avrami's parameters. K is the rate constant evaluated considering the nucleation and crystalline growth rates, and n is the Avrami exponent which is related with the crystallite geometry[37-40]. Nonisothermal crystallization data, acquired using constant cooling rates may be correlated through an expression formally identical to Avrami Equation 7:

$$Y = ln\left(ln\frac{1}{1-x}\right) = lnK' - n'ln\tau \quad (7)$$

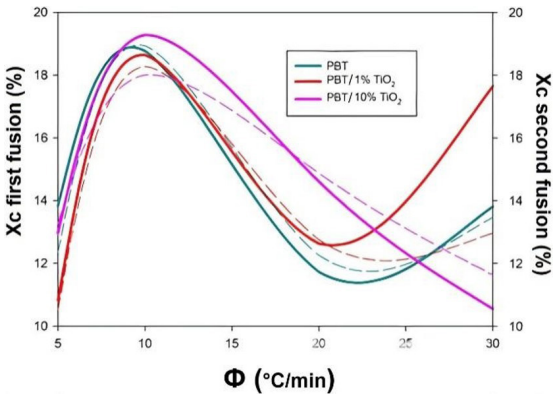

Figure 5. Plots for the crystallinity degree (Xc) developed during F1 (solid lines) and F2 (dashed lines). Compounds indicated.

Nevertheless, when using this model for nonisothermal crystallization investigations the parameters K' and n' are the heating rate ϕ functions, and not of temperature as in the Avrami model. Therefore, our researcher group has named Pseudo-Avrami[25,26].

The relative crystallinity of PBT and PBT/TiO_2 composites are displayed in Figure S9 which presents the theoretical (solid lines) and experimental (symbols) data. All plots displayed sigmoidal shapes characterizing continuous phase transition as commonly observed in polymers. Plots in Figure S9 present reasonable fits without huge deviation between the experimental and theoretical data. Only for PBT/10% TiO_2 cooled at 5 °C/min presented deviation at the end of the primary crystallization. It can be verified that the experimental relative crystallinity developed subtly higher than the theoretical predictions, in general, when using rates lower than 10 °C/min and higher than 20 °C/min higher deviations are computed, which may be linked to the noise and time-lag effects, additionally, for PBT/10% TiO_2 it is supposed to be also linked to the TiO_2 addition influence. Nevertheless, in general, Pseudo-Avrami described the crystallization of PBT and PBT/TiO_2 composites in

a reasonable mode. The sigmoids may be divided into three stages, i.e., the first stage due to the nucleation, the second stage due to the primary crystallization which takes place at an accelerated rate with a high amount of mass transformation, and the third stage due to the secondary crystallization that is slower and more prominent for the slower cooling rates. It is related to crystallite impingement when the crystallization is finishing[37,41].

As above verified for the crystallization rates, increasing the cooling rates displaced the sigmoids to higher times (lower temperatures), in general upon higher cooling rates the specimen crystallizes faster nevertheless the developed crystallites are shorter and/or imperfects, thus depending on the desired morphology the cooling rates may be a proper tool to attain it. As mentioned, the sigmoids may be divided into three stages, i.e., nucleation, primary crystallization, and secondary crystallization, related to the discrepancy between theoretical and experimental data the higher deviation was verified during the begging, $0 < X_{rel} < 10\%$ and the crystallization ending, i.e., $X_{rel} > 80\%$.

From the sigmoids presented in Figure S9 the Pseudo-Avrami plots were built and are presented in Figure 6, through the plots of Y versus ln τ according to Equation 6. Linearity deviation was mainly verified when the crystallization was beginning and when it was finishing as illustrated. Clearly, Pseudo-Avrami plots may be divided into three stages: 1st - nucleation, 2nd -primary crystallization, and 3rd - secondary crystallization, corroborating with presented data in Figure S9.

The discrepancy between theoretical and experimental data was measured and data are presented in Figure 7 for PBT/1% TiO_2. In general, the higher deviation was verified for higher cooling rates, and for the beginning and ending of crystallization as mentioned. Whether the analysis is concentered between $20\% < X_{rel} < 80\%$ the discrepancy goes down as demonstrated in Figure 7b, confirming Pseudo-Avrami fits quite well the crystallization from the melting of PBT and PBT/TiO_2 composites.

Figure 8 presents the crystallization rate constant (K') and maximum crystallization rate (C_{max}) as the cooling rate function for the investigated compounds, both parameters are related to the crystallization rate and through the displayed data they increased with the cooling rates, i.e., theoretical and experimental crystallization rates followed similar trend[26,42-45]. For a given cooling rate, the crystallization rate was higher for neat PBT indicating somehow TiO_2 decreased PBT's crystallizability, i.e., decreased PBT's ability to fast crystallize and hinder the transformation mechanisms, i.e., nucleation, primary and secondary crystallization, possibly changing the activation energy for the crystallization as further on investigated. In the Supplementary Material, in Table S2 the readers find the Pseudo-Avrami exponent and the R^2 parameter.

3.6 Mo and co-workers modeling

Mo and co-workers[45,46] developed a model to correlate non-isothermal crystallization parameters in polymers tested using constant cooling/heating rates, assuming the needed time τ to reach a given level of relative crystallinity due to the cooling/heating rate ϕ, according to Equation 8:

$$\phi = F\tau^{-\alpha} \tag{8}$$

where $F = F(x)$ and $\alpha = \alpha(x)$ are Mo's parameters, i.e., the rate constant and Mo exponent, respectively. Results acquired from the DSC peaks integration must be interpolated to have ϕ versus τ at constant x.

Mo parameters, for each relative crystallinity, are obtained by linear regression of the experimental data, according to Equation 9:

$$ln\phi = ln F - \alpha ln\tau \tag{9}$$

Figure S12c shows sigmoids for PBT/5% TiO_2 where symbols are the experimental data acquired during cooling, and the solid lines are the theoretical data computed according to Mo model. Plots presented quite good fits between experimental and theoretical data with subtle deviation at the crystallization extremes, i.e., beginning and ending, i.e., possibly linked with the nucleation and spherulites impingement, following a similar trend as already observed for Pseudo-Avrami model. From these sigmoids Mo plots

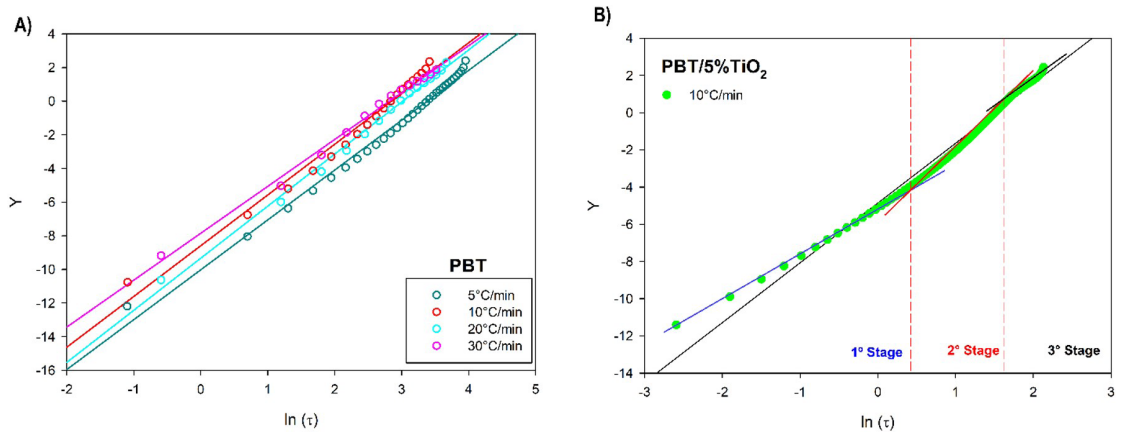

Figure 6. (A) Pseudo-Avrami plots of PBT built for the indicated cooling rates; (B) Pseudo-Avrami plots of PBT/5% TiO_2 cooled at 10 °C/min displaying crystallization in three stages.

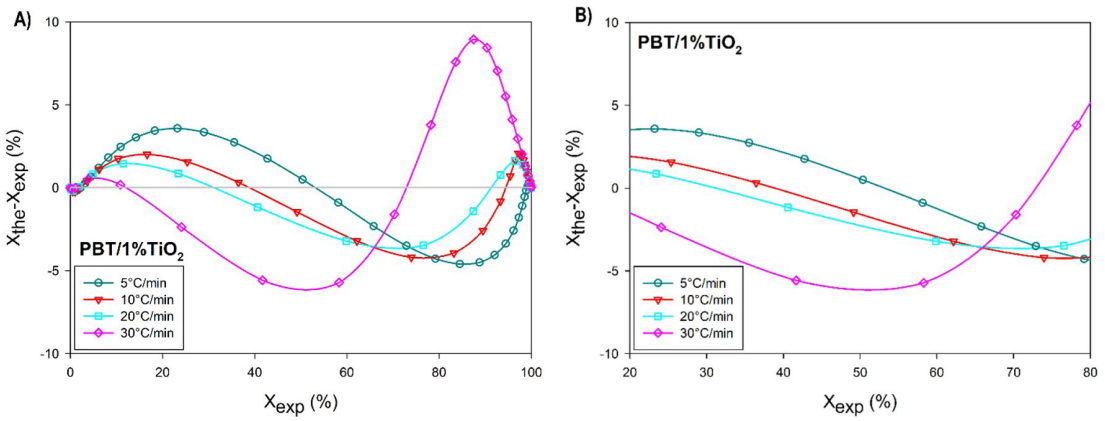

Figure 7. (A) Discrepancy for the whole melt crystallization of PBT/1%TiO2 at indicated cooling rates; (B) Discrepancy PBT/1%TiO_2 for the melt crystallization PBT/1%TiO2 between 20% < Xrel < 80% at indicated cooling rates. Plots built according to Pseudo-Avrami model.

were built and presented in Figure S11d for PBT/10% TiO_2 and 10% < X_{rel} < 90% from an overview of these data may be suggested Mo is adequate to modeling PBT and PBT/TiO_2 composites. Plots for other compounds are displayed in the Supplementary Material; please see the Figure S11 and Figure S12.

Figure 9 shows the discrepancy between the theoretical and experimental data for PBT/10%TiO_2 evaluated using Mo model, following a similar trend as already observed for Pseudo-Avrami. A huger deviation was observed at the beginning and end of crystallization, nevertheless if assumed the range 20 < X_{rel} < 80% the deviation is quite low, i.e., less than 5% which confirms Mo model describes very well the crystallization from the melt of PBT compounds[41,47].

Mo parameters F and α were measured using Equation 9 and are graphically presented in Figure 10[47,48]. In the Supplementary Material, Table S3 the readers find the R^2 parameter for the investigated compounds.

F increased with the degree of crystallization, i.e., for higher crystallinity much energy must be supplied to the system; a quite similar trend was observed for PP/PET blends as reported by Zhu et al.[49]. Related to TiO_2 addition, PBT composites displayed higher F suggesting that with the crystallization development the composites need much energy[50-52].

Mo exponent slowly increased with the degree of crystallinity suggesting crystalline structures more complexes were produced with the crystallization advance, i.e., nuclei are formed, as crystallization advance new macromolecules are added, progressing to the fibrils and then to the spherulites, which increase in size and can become more crystalline with the crystallization improvement, their crystallinity also depending on the applied crystallization parameters (time, temperature, cooling/heating rates), which can be used to control the whole crystallization. Parameters reported in the present paper may be used as proper tools to control the crystallization rate and the degree of crystallinity of PBT and PBT/TiO_2 composites.

The following section presents the calculations for the activation energy for the melt crystallization and for the fusions.

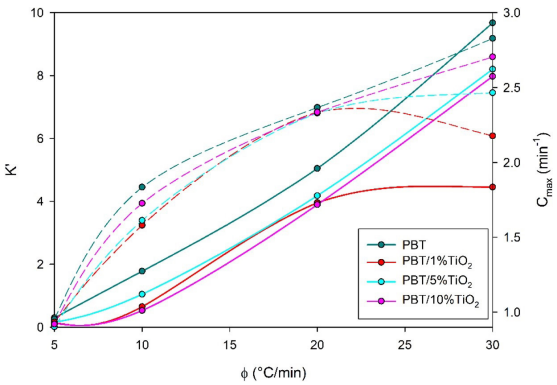

Figure 8. Pseudo-Avrami rate crystallization constant, K' (solid lines) and maximum crystallization rate, Cmax (dotted lines) as cooling rate function. Compounds indicated.

3.7 Activation Energy (E_a) – Melt crystallization

The conversion rate of a chemical reaction is commonly reported as the product of a temperature-dependent rate constant K(T) and a function of the f(x) conversion characteristic of the reaction mechanism, as shown in Equation 10:

$$\frac{dx}{dt} = K(T) f(x) \quad (10)$$

Isoconversional models are more applied to determine the activation energy of crystallizations. Friedman's model[53,54] is based on the logarithmic of the conversion rate assuming a constant rate K(T) defined by Arrhenius, which is shown in Equation 11:

$$k(T) = A exp^{-\frac{E_a}{RT}} \quad (11)$$

Where A is a pre-exponential factor constant and R = 8.314 J K^{-1} mol^{-1} is the universal gas constant.

Transformations from the amorphous/disordered state to the crystalline state in polymeric melt are considered

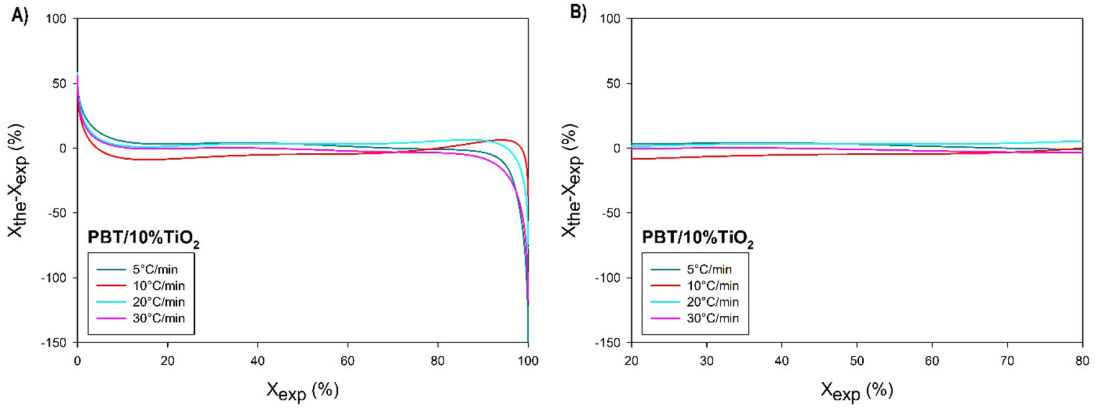

Figure 9. (A) Discrepancy between theoretical and experimental data for PBT/10%TiO_2 during the melt crystallization calculated using Mo model. Indicated cooling rates; (B) Discrepancy evaluated for 20 < Xrel < 80%.

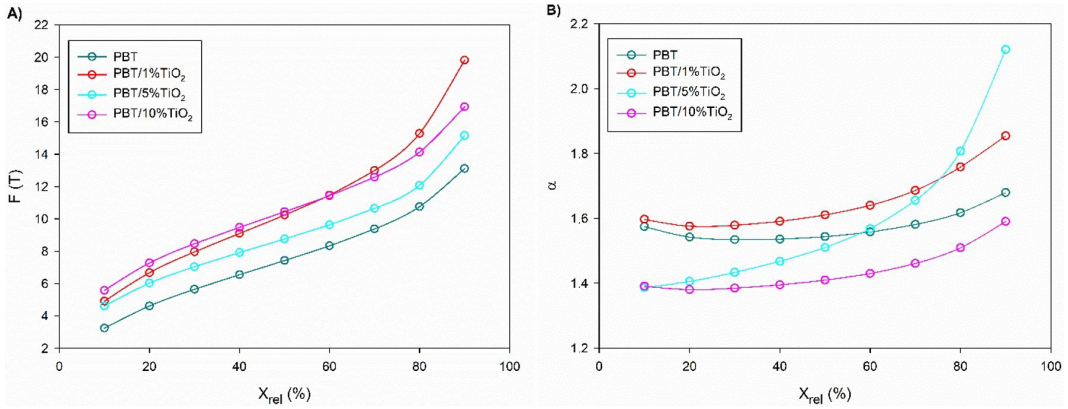

Figure 10. Mo parameters for the crystallization from the melt of PBT compounds. (A) F (T) and (B) Mo exponent α.

complex reactions; therefore Equations 10 and 11 must be generalized to:

$$\frac{dx}{dt} = A\exp^{-\frac{E_a(x)}{RT}} f(x) \quad (12)$$

Generally, E_a is a function of conversion (in this case it is a function of (X_{rel}) and Equation 12 can be converted to the logarithmic form:

$$ln\left(\frac{dx}{dt}\right) = ln\left[A.f(x)\right] - \frac{E_a(x)}{RT} \quad (13)$$

For a relative crystallinity $x = X_{rel}$, the plot of $ln\left(\frac{dx}{dt}\right)$ x $\frac{1000}{T}$ acquired from data computed at different cooling rates generates a straight line with slope $\frac{E_a}{R}$, this treatment repeated for the different values of X_{rel} results in E_a as function of X_{rel}. This method was applied in this work for X_{rel} ranging between 0 and 1.0 as shown in Figure 11.

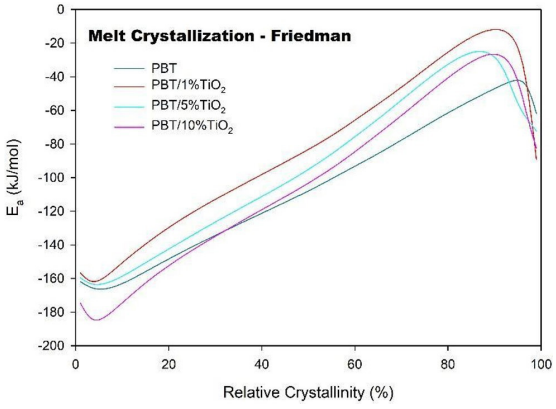

Figure 11. E_a for the crystallization from the melt of PBT compounds measured using the Friedman isoconversional method. Compositions indicated.

As can be seen from Figure 11, all activation energies are negative, indicating that energy has to be removed from the system in order to promote the melt crystallization. Considering the absolute values of the activation energies, less energy has to be removed from the system for the TiO_2/PBT compounds when compared to neat PBT. The only

exception from this behavior is the composition with 10% TiO_2 load in the range 0-30% of relative crystallinity, which could be attributed to a measurement error. The fact that all the curves of E_a versus X_{rel} show up as almost parallel lines indicates that there is no significant change in the melt crystallization mechanism when adding the TiO_2. The effect of filler is also nonlinear. A quite similar nonlinear shifting of activation energy curves was reported by Ries et al.[55] for the cold and melt crystallization of PHB/ZnO composites.

3.8 Activation energy (E_a) – First fusion

In contrast to crystallization kinetics, fusion kinetics has been rarely investigated[56]. Few studies report polymer fusion kinetics by means of isoconversional kinetic models[57-59]. A differential or integral isoconversional method may be applied depending on the nature of the experimental data. If the reported data are from DSC measurements, therefore, Friedman's differential isoconversional method[53,54] may be used.

Toda et al.[20,60] proposed a nucleation model for polymer fusion which fusion starts with melting the cylindrical cores. However, Friedman's isoconversional model is powerful to study the fusion kinetics and evaluate E_a under superheating[61]. In those situations, a decrease in s of the fusions upon temperature increase is expected[62]. This behavior was mostly observed in this work.

The numerical optimization method[63] is based on the data of Friedman analytical method. The acquired data from the Friedman method such as E(x) and A(x) are numerically optimized, the best fit between the experimental plots is obtained through non-linear optimization based on the least squares method. For fusion, this model-free method was the most suitable in this work, due to the better R^2 of the analytical plot, which ranged from 0,932 to 0,996. E_as were computed using the numerical optimization method and plotted as molten fraction function. Figure 12 shows E_a for the first fusion of PBT and PBT/TiO_2 composites. Neat PBT fusion requires the highest activation energy; while the lowest $E_a$was observed for PBT/1%TiO_2 then a further increase in filler content raises the activation energy again. This behavior is similarly nonlinear as the trend verified for the melt crystallization.

3.9 Activation energy (E_a) – Second fusion

E_a for the second fusion of investigated compounds was measured using the numerical optimization method, similarly to the first fusion. This method based on the Friedman model presented quite high R^2, i.e., $0,975 < R^2 < 0,996$. Plots are presented in the Supplementary Material, please see Figure S14.

Acquired E_a*s* are plotted as molten fraction (X_m) function and shown in Figure 13. All investigated compounds presented a similar profile, i.e., E_a decreased upon the fusion advance, the only exception observed was an increase in for $X_m > 95\%$ until the end of fusion. In the final stages of the second fusion, the verified trend for E_a was: $E_{95\%PBT} > E_{90\%PBT} > E_{99\%PBT} > E_{100\%PBT}$. During the second melting, there were no significant variations in E_a with TiO_2 addition

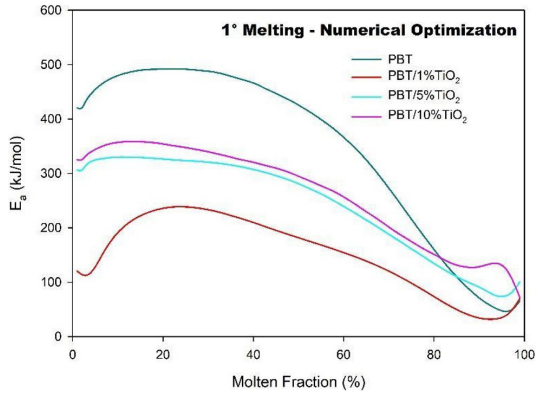

Figure 12. E_a for the first fusion of PBT and PBT/TiO_2 composites using the numerical optimization method

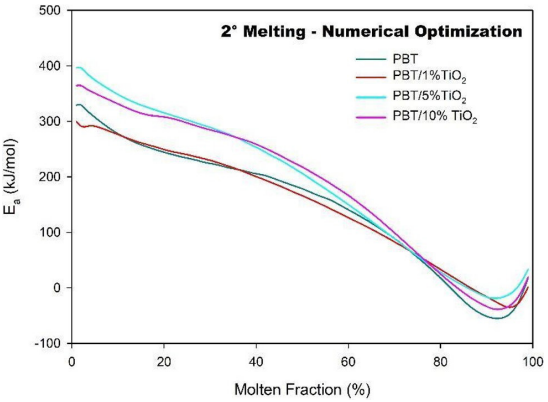

Figure 13. E_a for the second fusion of PBT and PBT/TiO_2 composites using the numerical optimization method.

and similarly to the first melting, there was no linear trend between TiO_2 and the computed E_a.

From Figure 12 and Figure 13 it may be verified that the second fusion character is quite different from the first one, as the first fusion is related to the quenched material from the mixing while the second fusion is related with the melt crystallized material, hence the second fusion was computed during the second heating with different thermal history and mainly distinct morphology altogether would be conducting to different activation energy as displayed in Figure 13.

4. Conclusions

PBT/TiO_2 compounds were successfully melting mixed; according to SEM images, TiO_2 nanoparticles are well dispersed in the PBT matrix without evidence of agglomeration. The melt crystallization, fusions, and activation energy (E_a) were evaluated based on DSC scans. Upon the integration of the DSC scans, the thermal events were visualized as sigmoids, indicating continuous phase transformation. Higher cooling rates shifted the sigmoides of the melt

crystallization to lower temperatures, while the fusions were almost insensible to the heating rates. Pseudo-Avrami and Mo models fit the melt crystallization kinetics quite well with subtle deviation only verified at the beginning and end of the crystallization, nevertheless quite high R^2 parameters were acquired. Standard negative activation energies were computed for the melt crystallization and positive activation energies for the fusions; the Friedman model was applied to both phase transition evaluations and high R^2 values suggest that they are a proper methodology. As expected, the activation energies decrease upon temperature increase for all filler contents.

5. Author's Contribution

- **Conceptualization** – José Vinícius Melo Barreto; Renate Maria Ramos Wellen.
- **Data curation** – José Vinícius Melo Barreto; Amanda Meneses Araújo; Antônio Anderson da Silva Gomes.
- **Formal analysis** – José Vinícius Melo Barreto; Amanda Meneses Araújo; Antônio Anderson da Silva Gomes.
- **Funding acquisition** - Renate Maria Ramos Wellen.
- **Investigation** – José Vinícius Melo Barreto; Amanda Meneses Araújo; Antônio Anderson da Silva Gomes.
- **Methodology** – Renate Maria Ramos Wellen.
- **Project administration** – Renate Maria Ramos Wellen.
- **Resources** – Renate Maria Ramos Wellen.
- **Software** – José Vinícius Melo Barreto; Amanda Meneses Araújo; Antônio Anderson da Silva Gomes.
- **Supervision** – Renate Maria Ramos Wellen.
- **Validation** – Renate Maria Ramos Wellen; Andreas Ries.
- **Visualization** – Renate Maria Ramos Wellen; Andreas Ries.
- **Writing – original draft** – José Vinícius Melo Barreto; Amanda Meneses Araújo; Antônio Anderson da Silva Gomes; Renate Maria Ramos Wellen.
- **Writing – review & editing** – Renate Maria Ramos Wellen; Andreas Ries; Janetty Jany Pereira Barros.

6. Acknowledgements

The authors acknowledge to the financial support from the Conselho Nacional de Desenvolvimento Científico e Tecnológico (CNPq) and from the Federal University of Paraíba (PIF13111-2020) Professor Renate Wellen is CNPq fellow (Number: 303426/2021-7). The authors thank to Olin Corporation (Brazil) for kindly supplying the reactants.

7. References

1. Wu, T., Hu, H. L., Du, Y. P., Jiang, D., & Yu, B. H. (2014). Discrimination of thermoplastic polyesters by MALDI-TOF MS and Py-GC/MS. *IJPAC. International Journal of Polymer Analysis and Characterization*, *19*(5), 441-452. http://dx.doi.org/10.1080/1023666X.2014.920126.
2. Szostak, M. (2004). Mechanical and thermal properties of PET/PBT blends. *Molecular Crystals and Liquid Crystals (Philadelphia, Pa.)*, *416*(1), 209-215. http://dx.doi.org/10.1080/15421400490481377.
3. Park, C.-S., Lee, K.-J., Nam, J.-D., & Kim, S.-W. (2000). Crystallization kinetics of glass fiber reinforced PBT composites. *Journal of Applied Polymer Science*, *78*(3), 576-585. http://dx.doi.org/10.1002/1097-4628(20001017)78:3<576::AID-APP120>3.0.CO;2-M.
4. Almeida, A., Nébouy, M., & Baeza, G. P. (2019). Bimodal crystallization kinetics of PBT/PTHF segmented block copolymers: impact of the chain rigidity. *Macromolecules*, *52*(3), 1227-1240. http://dx.doi.org/10.1021/acs.macromol.8b01689.
5. Deshmukh, G. S., Peshwe, D. R., Pathak, S. U., & Ekhe, J. D. (2014). Nonisothermal crystallization kinetics and melting behavior of poly(butylene terephthalate)(PBT) composites based on different types of functional fillers. *Thermochimica Acta*, *581*, 41-53. http://dx.doi.org/10.1016/j.tca.2014.02.007.
6. Lehmann, B., & Karger-Kocsis, J. (2009). Isothermal and non-isothermal crystallisation kinetics of pCBT and PBT. *Journal of Thermal Analysis and Calorimetry*, *95*(1), 221-227. http://dx.doi.org/10.1007/s10973-007-8939-1.
7. Kulshreshtha, B., Ghosh, A. K., & Misra, A. (2003). Crystallization kinetics and morphological behavior of reactively processed PBT/epoxy blends. *Polymer*, *44*(16), 4723-4734. http://dx.doi.org/10.1016/S0032-3861(03)00347-1.
8. Kalkar, A. K., Deshpande, V. D., & Purkar, B. R. (2018). Evaluation of thermal transitions in Poly(butylene terephthalate)/15A MMT nanocomposites: nonisothermal experiments and modelling using isoconversional methods. *Thermochimica Acta*, *660*, 23-36. http://dx.doi.org/10.1016/j.tca.2017.12.005.
9. Jiang, L., Huang, Z., Wang, X., Lai, M., Zhang, Y., & Zhou, H. (2020). Influence of reactive compatibilization on the mechanical, thermal and rheological properties of highly filled PBT/Al2O3 composites. *Materials & Design*, *196*, 109175. http://dx.doi.org/10.1016/j.matdes.2020.109175.
10. Cao, Y., Xu, P., Wu, B., Hoch, M., Lemstra, P. J., Yang, W., Dong, W., Du, M., Liu, T., & Ma, P. (2020). High-performance and functional PBT/EVMG/CNTs nanocomposites from recycled sources by in situ multistep reaction-induced interfacial control. *Composites Science and Technology*, *190*, 108043. http://dx.doi.org/10.1016/j.compscitech.2020.108043.
11. Tekin, D., Birhan, D., & Kiziltas, H. (2020). Thermal, photocatalytic, and antibacterial properties of calcinated nano-TiO2/polymer composites. *Materials Chemistry and Physics*, *251*, 123067. http://dx.doi.org/10.1016/j.matchemphys.2020.123067.
12. Deshmukh, G. S., Peshwe, D. A., Pathak, S. U., & Ekhe, J. D. (2011). A study on effect of mineral additions on the mechanical, thermal, and structural properties of poly(butylene terephthalate)(PBT) composites. *Journal of Polymer Research*, *18*(5), 1081-1090. http://dx.doi.org/10.1007/s10965-010-9510-5.
13. Wang, S., & Zhang, J. (2014). Effect of titanium dioxide (TiO2) on largely improving solar reflectance and cooling property of high density polyethylene (HDPE) by influencing its crystallization behavior. *Journal of Alloys and Compounds*, *617*, 163-169. http://dx.doi.org/10.1016/j.jallcom.2014.07.191.
14. Supaphol, P., Thanomkiat, P., Junkasem, J., & Dangtungee, R. (2007). Non-isothermal melt-crystallization and mechanical properties of titanium (IV) oxide nanoparticle-filled isotactic polypropylene. *Polymer Testing*, *26*(1), 20-37. http://dx.doi.org/10.1016/j.polymertesting.2006.07.011.
15. Yang, T.-C., Noguchi, T., Isshiki, M., & Wu, J.-H. (2014). Effect of titanium dioxide on chemical and molecular changes in PVC sidings during QUV accelerated weathering. *Polymer Degradation & Stability*, *104*, 33-39. http://dx.doi.org/10.1016/j.polymdegradstab.2014.03.023.
16. Scuderi, V., Buccheri, M. A., Impellizzeri, G., Di Mauro, A., Rappazzo, G., Bergum, K., Svensson, B. G., & Privitera, V. (2016). Photocatalytic and antibacterial properties of titanium dioxide flat film. *Materials Science in Semiconductor Processing*, *42*(Part 1), 32-35. http://dx.doi.org/10.1016/j.mssp.2015.09.005.
17. Olmos, D., Domínguez, C., Castrillo, P. D., & Gonzalez-Benito, J. (2009). Crystallization and final morphology of HDPE: effect of the high energy ball milling and the presence of

TiO_2 nanoparticles. *Polymer*, *50*(7), 1732-1742. http://dx.doi.org/10.1016/j.polymer.2009.02.011.

18. Zhou, G., Li, L., Jiang, M., Wang, G., Wang, R., Wu, G., & Zhou, G. (2021). Renewable poly(butene 2, 5-furan dicarboxylate) nanocomposites constructed by TiO_2 nanocubes: synthesis, crystallization, and properties. *Polymer Degradation & Stability*, *189*, 109591. http://dx.doi.org/10.1016/j.polymdegradstab.2021.109591.
19. Friedman, H. L. (1964). Kinetics of thermal degradation of char-forming plastics from thermogravimetry: application to a phenolic plastic. *Journal of Polymer Science Part C: Polymer Symposia*, *6*(1), 183-195. http://dx.doi.org/10.1002/polc.5070060121.
20. Toda, A., Hikosaka, M., & Yamada, K. (2002). Superheating of the melting kinetics in polymer crystals: a possible nucleation mechanism. *Polymer*, *43*(5), 1667-1679. http://dx.doi.org/10.1016/S0032-3861(01)00733-9.
21. Christakopoulos, F., Troisi, E. M., Sologubenko, A. S., Friederichs, N., Stricker, L., & Tervoort, T. A. (2021). Melting kinetics, ultra-drawability and microstructure of nascent ultra-high molecular weight polyethylene powder. *Polymer*, *222*, 123633. http://dx.doi.org/10.1016/j.polymer.2021.123633.
22. Monteiro, A. E. G. (2020). *Desenvolvimento de compósitos poliméricos de poli (butileno adipatoco-tereftalato)(PBAT)/óxido de zinco (ZnO) e poli (butileno adipato-cotereftalato) (PBAT)/dióxido de titânio (TiO_2)* (Doctoral thesis). Universidade Federal de Pernambuco, Recife.
23. Conix, A., & Van Kerpel, R. (1959). Crystallization behavior and melting properties of m-phenylene group containing polyesters. *Journal of Polymer Science*, *40*(137), 521-532. http://dx.doi.org/10.1002/pol.1959.1204013720.
24. Silva, I. D. S., Jaques, N. G., Barbosa, M. C., No., Agrawal, P., Ries, A., Wellen, R. M. R., & Canedo, E. L. (2018). Melting and crystallization of PHB/ZnO compounds. *Journal of Thermal Analysis and Calorimetry*, *132*(1), 571-580. http://dx.doi.org/10.1007/s10973-017-6749-7.
25. Wellen, R. M. R., Canedo, E. L., & Rabello, M. S. (2015). Melting and crystallization of poly(3-hydroxybutyrate)/carbon black compounds: effect of heating and cooling cycles on phase transition. *Journal of Materials Research*, *30*(21), 3211-3226. http://dx.doi.org/10.1557/jmr.2015.287.
26. Vitorino, M. B. C., Cipriano, P. B., Wellen, R. M. R., Canedo, E. L., & Carvalho, L. H. (2016). Nonisothermal melt crystallization of PHB/babassu compounds. *Journal of Thermal Analysis and Calorimetry*, *126*(2), 755-769. http://dx.doi.org/10.1007/s10973-016-5514-7.
27. Groeninckx, G., Reynaers, H., Berghmans, H., & Smets, G. (1980). Morphology and melting behavior of semicrystalline poly(ethylene terephthalate). I. Isothermally crystallized PET. *Journal of Polymer Science. Polymer Physics Edition*, *18*(6), 1311-1324. http://dx.doi.org/10.1002/pol.1980.180180612.
28. Cruz, L. C. A. (2013). *Estudo da cinética de cristalização do Polifluoreto de vinilideno (PVDF)* (Doctoral thesis). Universidade Federal do Rio de Janeiro, Rio de Janeiro.
29. Wellen, R. M. R., Rabello, M. S., Araujo, I. C., Jr., Fechine, G. J. M., & Canedo, E. L. (2015). Melting and crystallization of poly(3-hydroxybutyrate): effect of heating/cooling rates on phase transformation. Polímeros. *Polímeros*, *25*(3), 296-304. http://dx.doi.org/10.1590/0104-1428.1961.
30. Bogoeva-Gaceva, G., Janevski, A., & Grozdanov, A. (1998). Crystallization and melting behavior of iPP studied by DSC. *Journal of Applied Polymer Science*, *67*(3), 395-404. http://dx.doi.org/10.1002/(SICI)1097-4628(19980118)67:3<395::AID-APP2>3.0.CO;2-H.
31. Fakirov, S., Fischer, E. W., Hoffmann, R., & Schmidt, G. F. (1977). Structure and properties of poly(ethylene terephthalate) crystallized by annealing in the highly oriented state: 2. Melting behaviour and the mosaic block structure of the crystalline layers. *Polymer*, *18*(11), 1121-1129. http://dx.doi.org/10.1016/0032-3861(77)90105-7.
32. Liu, M., Zhao, Q., Wang, Y., Zhang, C., Mo, Z., & Cao, S. (2003). Melting behaviors, isothermal and non-isothermal crystallization kinetics of nylon 1212. *Polymer*, *44*(8), 2537-2545. http://dx.doi.org/10.1016/S0032-3861(03)00101-0.
33. Bassett, D. C. (1981). *Principles of polymer morphology*. Cambridge: Cambridge University Press.
34. Avrami, M. (1941). Granulation, phase change, and microstructure kinetics of phase change. III. *The Journal of Chemical Physics*, *9*(2), 177-184. http://dx.doi.org/10.1063/1.1750872.
35. Avrami, M. (1940). Kinetics of phase change. II transformation-time relations for random distribution of nuclei. *The Journal of Chemical Physics*, *8*(2), 212-224. http://dx.doi.org/10.1063/1.1750631.
36. Avrami, M. (1939). Kinetics of phase change. I General theory. *The Journal of Chemical Physics*, *7*(12), 1103-1112. http://dx.doi.org/10.1063/1.1750380.
37. Coutinho, S. V. C. R., Barros, A. B. S., Barros, J. J. P., Albuquerque, A. K. C., Barreto, J. V. M., Siqueira, D. D., Ries, A., & Wellen, R. M. R. (2021). On the nonisothermal melt crystallization kinetics of industrial batch crosslinked polyethylene. *Journal of Applied Polymer Science*, *138*(33), 50807. http://dx.doi.org/10.1002/app.50807.
38. Chuah, K. P., Gan, S. N., & Chee, K. K. (1999). Determination of Avrami exponent by differential scanning calorimetry for non-isothermal crystallization of polymers. *Polymer*, *40*(1), 253-259. http://dx.doi.org/10.1016/S0032-3861(98)00188-8.
39. Wellen, R. M. R., & Canedo, E. L. (2016). Nonisothermal melt and cold crystallization kinetics of poly(3-hydroxybutyrate) and poly(3-hydroxybutyrate)/carbon black compounds: evaluation of Pseudo-Avrami, Ozawa, and Mo models. *Journal of Materials Research*, *31*(6), 729-739. http://dx.doi.org/10.1557/jmr.2016.68.
40. Drzewicz, A., Juszyńska-Gałązka, E., Zając, W., Piwowarczyk, M., & Drzewiński, W. (2020). Non-isothermal and isothermal cold crystallization of glass-forming chiral smectic liquid crystal (S)-4′-(1-methyloctyloxycarbonyl) biphenyl-4-yl 4-[7-(2, 2, 3, 3, 4, 4, 4-heptafluorobutoxy) heptyl-1-oxy]-benzoate. *Journal of Molecular Liquids*, *319*, 114153. http://dx.doi.org/10.1016/j.molliq.2020.114153.
41. Schäfer, H., Reul, L. T. A., Souza, F. M., Wellen, R. M. R., Carvalho, L. H., Koschek, K., & Canedo, E. L. (2021). Crystallization behavior of polycaprolactone/babassu compounds. *Journal of Thermal Analysis and Calorimetry*, *143*(4), 2963-2972. http://dx.doi.org/10.1007/s10973-020-09433-0.
42. Canedo, E. L., Wellen, R. M. R., & Almeida, Y. M. B. (2016). *Cristalização de Polímeros–Tratamento de Dados e Modelagem Macrocinética*. Brazil: Programa de Recursos Humanos da ANP – PRH28/UFPE.
43. Song, L., & Qiu, Z. (2009). Crystallization behavior and thermal property of biodegradable poly(butylene succinate)/functional multi-walled carbon nanotubes nanocomposite. *Polymer Degradation & Stability*, *94*(4), 632-637. http://dx.doi.org/10.1016/j.polymdegradstab.2009.01.009.
44. Zou, P., Tang, S., Fu, Z., & Xiong, H. (2009). Isothermal and non-isothermal crystallization kinetics of modified rape straw flour/high-density polyethylene composites. *International Journal of Thermal Sciences*, *48*(4), 837-846. http://dx.doi.org/10.1016/j.ijthermalsci.2008.06.010.
45. Liu, T., Mo, Z., & Zhang, H. (1998). Nonisothermal crystallization behavior of a novel poly(aryl ether ketone): PEDEKmK. *Journal of Applied Polymer Science*, *67*(5), 815-821. http://dx.doi.

org/10.1002/(SICI)1097-4628(19980131)67:5<815::AID-APP6>3.0.CO;2-W.

46. Liu, T., Mo, Z., Wang, S., & Zhang, H. (1997). Nonisothermal melt and cold crystallization kinetics of poly(aryl ether ether ketone ketone). *Polymer Engineering and Science*, *37*(3), 568-575. http://dx.doi.org/10.1002/pen.11700.
47. Li, C., & Dou, Q. (2014). Non-isothermal crystallization kinetics and spherulitic morphology of nucleated poly(lactic acid): effect of dilithium hexahydrophthalate as a novel nucleating agent. *Thermochimica Acta*, *594*, 31-38. http://dx.doi.org/10.1016/j.tca.2014.08.036.
48. Mohtaramzadeh, Z., Hemmati, F., Kasbi, S. F., Goodarzi, V., Arnhold, K., & Khonakdar, H. A. (2020). Structure-properties correlations in poly(ε-caprolactone)/poly(styrene-co-acrylonitrile)/nanosilica mixtures: interrelationship among phase behavior, morphology and non-isothermal crystallization kinetics. *Polymer Testing*, *89*, 106593. http://dx.doi.org/10.1016/j.polymertesting.2020.106593.
49. Zhu, Y., Liang, C., Bo, Y., & Xu, S. (2015). Non-isothermal crystallization behavior of compatibilized polypropylene/recycled polyethylene terephthalate blends. *Journal of Thermal Analysis and Calorimetry*, *119*(3), 2005-2013. http://dx.doi.org/10.1007/s10973-014-4349-3.
50. Qiu, Z. B., Zhou, H. W., Mo, Z. S., Zhang, H. F., & Wu, Z. W. (2000). Nonisothermal cold crystallization kinetics of Poly(aryl ether diphenyl ether ketone). *Polymer Journal*, *32*(3), 287-290. http://dx.doi.org/10.1295/polymj.32.287.
51. Liu, F., Shan, X., & Wang, Z. (2020). Nonisothermal crystallization behaviors of ethylene–acrylic acid copolymer and ethylene–acrylic acid copolymer/chloroprene rubber thermoplastic vulcanizate. *Journal of Thermoplastic Composite Materials*, *35*(10), 1548-1560. http://dx.doi.org/10.1177/0892705720939138.
52. Xiuju, Z., Juncai, S., Huajun, Y., Zhidan, L., & Shaozao, T. (2011). Mechanical properties, morphology, thermal performance, crystallization behavior, and kinetics of PP/microcrystal cellulose composites compatibilized by two different compatibilizers. *Journal of Thermoplastic Composite Materials*, *24*(6), 735-754. http://dx.doi.org/10.1177/0892705711403527.
53. Deb, P. (2014). *Kinetics of heterogeneous solid state processes*. India: Springer. http://dx.doi.org/10.1007/978-81-322-1756-5.
54. Vyazovkin, S., & Wight, C. A. (1998). Isothermal and non-isothermal kinetics of thermally stimulated reactions of solids. *International Reviews in Physical Chemistry*, *17*(3), 407-433. http://dx.doi.org/10.1080/014423598230108.
55. Ries, A., Canedo, E. L., Souto, C. R., & Wellen, R. M. R. (2016). Non-isothermal cold crystallization kinetics of poly(3-hydoxybutyrate) filled with zinc oxide. *Thermochimica Acta*, *637*, 74-81. http://dx.doi.org/10.1016/j.tca.2016.06.002.
56. Liavitskaya, T., Birx, L., & Vyazovkin, S. (2017). Melting kinetics of superheated crystals of glucose and fructose. *Physical Chemistry Chemical Physics*, *19*(38), 26056-26064. http://dx.doi.org/10.1039/C7CP05486F. PMid:28926042.
57. Vyazovkin, S., Yancey, B., & Walker, K. (2013). Nucleation-Driven Kinetics of Poly(ethylene terephthalate) Melting. *Macromolecular Chemistry and Physics*, *214*(22), 2562-2566. http://dx.doi.org/10.1002/macp.201300443.
58. Vyazovkin, S., & Sbirrazzuoli, N. (2006). Isoconversional Kinetic Analysis of Thermally Stimulated Processes in Polymers. *Macromolecular Rapid Communications*, *27*(18), 1515-1532. http://dx.doi.org/10.1002/marc.200600404.
59. Vyazovkin, S. (2017). Isoconversional kinetics of polymers: the decade past. *Macromolecular Rapid Communications*, *38*(3), 1600615. http://dx.doi.org/10.1002/marc.201600615. PMid:28009078.
60. Toda, A., Kojima, I., & Hikosaka, M. (2008). Melting kinetics of polymer crystals with an entropic barrier. *Macromolecules*, *41*(1), 120-127. http://dx.doi.org/10.1021/ma702162m.
61. Christakopoulos, F., Troisi, E., & Tervoort, T. A. (2020). Melting kinetics of nascent Poly(tetrafluoroethylene) powder. *Polymers*, *12*(4), 791. http://dx.doi.org/10.3390/polym12040791. PMid:32252294.
62. Vyazovkin, S. (2020). Activation energies and temperature dependencies of the rates of crystallization and melting of polymers. *Polymers*, *12*(5), 1070. http://dx.doi.org/10.3390/polym12051070. PMid:32392771.
63. Radojević, M., Janković, B., Jovanović, V., Stojiljković, D., & Manić, N. (2018). Comparative pyrolysis kinetics of various biomasses based on model-free and DAEM approaches improved with numerical optimization procedure. *PLoS One*, *13*(10), e0206657. http://dx.doi.org/10.1371/journal.pone.0206657. PMid:30379972.

Received: Sept. 19, 2022
Revised: Feb. 14, 2023
Accepted: Feb. 20, 2023

Supplementary Material

Supplementary material accompanies this paper.

Figure S1. Typical DSC scan for PBT, collected during applied thermal cycles for the heating/cooling/re-heating of 10 °C/min. Dotted red line is the applied thermal program. Solid blue line the heat flow signal with the investigated phase transitions, i.e., F_1.

Figure S2. The half melt crystallization time $\tau_{1/2}$ (dashed line) and melt crystallization rate (solid line) of produced compounds as function of tested cooling rates.

Figure S3. Relative crystallinity (solid line) and Crystallization rate (dotted line) as temperature function. Compounds and cooling rates indicated.

Figure S4. Relative crystallinity (solid line) and Crystallization rate (dotted line) as temperature function. Compounds and cooling rates indicated.

Figure S5. Molten fraction (solid line) and Melting rates (dotted line) as temperature function of F_1. Compounds and cooling rates indicated.

Figure S6. Molten fraction (solid line) and Melting rates (dotted line) as temperature function of F_2. Compounds and cooling rates indicated.

Figure S7. Pseudo-Avrami plots of neat and PBT/TiO_2 cooled at indicated cooling rates illustrating crystallization development in three stages.

Figure S8. Pseudo-Avrami plots of composites a) PBT/1%TiO_2, b) PBT/5%TiO_2 and c) PBT/10%TiO_2 computed for the indicated cooling rates.

Figure S9. Relative crystallinity of a) neat PBT, b) PBT/1%TiO_2, c) PBT/5%TiO_2 and d) PBT/10%TiO_2 at displayed cooling rates. The theoretical data are solid lines and the experimental are symbols.

Figure S10. Discrepancy for the whole melt crystallization of a) neat polymer, b) PBT/5%TiO_2 and c) PBT/10%TiO_2 at indicated cooling rates. And Discrepancy for the melt crystallization between 20% < X_{rel} < 80% of d) neat polymer, e) PBT/5%TiO_2 and f) PBT/10%TiO_2. Plots built according to Pseudo-Avrami model.

Figure S11. Mo plots for the melt crystallization of a) neat PBT, b) PBT with 1%TiO_2, c) PBT/5%TiO_2, and d) PBT/10%TiO_2 at indicated degree of crystallinity.

Figure S12. Relative crystallinity for the melt crystallization of a) neat PBT, b) PBT/1%TiO_2, c) PBT/5%TiO_2, and d) PBT/10%TiO_2 at indicated cooling rates.

Figure S13. Deviation between theoretical and experimental data during the melt crystallization evaluated using Mo model (cooling rates indicated) of a) neat PBT, b) PBT/1%TiO_2 and c) PBT/5%TiO_2. And discrepancy evaluated for 0 < X_{rel} < 80% of d) neat PBT, e) PBT/1%TiO_2 and f)

PBT/5%TiO_2.

Figure S14. for the second fusion of PBT and PBT/TiO_2 composites using the numerical optimization method

Table S1. Melt crystallization data for indicated compositions and rates.

Table S2. Pseudo-Avrami expoent (n'), R^2 and degree of crystallinity (X_c %) for the investigated compounds.

Table S3. R^2 parameter for Mo fits computed for the investigated compounds.

Table S4. Data for the first fusion for PBT and PBT/TiO_2 composites.

Table S5. Data for the second fusion for PBT and PBT/TiO_2 composites.

This material is available as part of the online article from https://doi.org/10.1590/0104-1428.20220087